4-1-2009

Integrated Reliability and Sizing Optimization of a Large Composite Structure

Christopher D. Eamon
Mississippi State University, Starkville, MS, christopher.eamon@wayne.edu

Masoud Rais-Rohani
Mississippi State University, Starkville, MS

Integrated Reliability and Sizing Optimization of a Large Composite Structure

Christopher D. Eamon[1] and Masoud Rais-Rohani[2]
Mississippi State University, Mississippi State, MS 39762

Abstract

In this paper, we present the application of probabilistic design modeling and reliability-based design optimization (RBDO) methodology to the sizing optimization of a composite advanced submarine sail structure under parametric uncertainty. With the help of probabilistic sensitivity analysis, the influence of individual random variables on each structural failure mode is examined, and the critical modes are treated as probabilistic design constraints under consistent lower bounds on the corresponding reliability indices. Whereas the failure modes are applied to structural components in the solution of the RBDO problem, the overall system reliability is also evaluated as a post-optimization step. The results indicate that in comparison to a deterministic optimum design, the structural mass of the probabilistic optimum design is slightly higher when consistent probabilistic constraints are imposed, and the overall structural stiffness is found to be more critical than individual component laminate ply thicknesses in meeting the specified design constraints. Moreover, the post-optimality analysis shows that the overall system failure probability of the probabilistic optimum design is more than 50% lower than that of the deterministic optimal design with less than 5% penalty in structural mass.

---

[1]Associate Professor, Department of Civil and Environmental Engineering, Eamon@engr.msstate.edu
[2]Professor, Department of Aerospace Engineering, Masoud@ae.msstate.edu

Introduction

Probabilistic modeling and reliability-based design optimization (RBDO) have gained broad recognition in recent years as an appropriate approach for structural optimization under uncertainty. In RBDO, a traditional deterministic structural optimization problem is replaced by a non-deterministic one subject to a combined set of deterministic and reliability-based (probabilistic) design constraints, with a parameter set that includes design as well as random variables. The resulting nonlinear, probabilistic mathematical programming problem is solved for the optimal values of design variables that improve a structural response of interest while considering the uncertainty in material, loading, sizing, and other contributing factors.

The evaluation of failure probability or associated reliability index for each reliability-based constraint poses a computational challenge in RBDO as the calculation of component reliability generally requires the solution of a separate optimization problem (in random-variable space) within, often larger, main design optimization problem (in design-variable space). When the evaluation of each limit state function is based on the finite element analysis (FEA) of a complex structural system, the RBDO problem becomes considerably more complicated and computationally intensive.

A significant body of RBDO related research exists and continues to grow, though a review of the many proposed RBDO formulations is beyond the scope of this paper. Despite the advancements in this area, few RBDO approaches applied specifically to ship structures appear in the technical literature. Some of these include Pu et al. (1997), Leheta et al. (1997), and Brown et al. (1996). Others have considered the reliability analysis of submarine structures without optimization (Morandi et al. 1994), or considered structural optimization without probabilistic analysis (Jang et al. 2003).

In this paper, an RBDO algorithm is presented and applied to a complex structural system representing an advanced submarine sail design made of glass-reinforced polymer composite materials. The results of RBDO problem for different combinations of component reliability constraints are examined, followed by a sensitivity analysis and the post-optimization assessment of the system reliability.

Structural Reliability

Given a limit state function, g in structural reliability analysis, it is desired to find the probability P that g is less than zero, for which a failure is indicated by

$$P_f = P\left[g(\boldsymbol{X}) < 0\right] \tag{1}$$

Probability of failure P_f is theoretically found by integrating the joint probability density function (PDF) over the failure region in the probabilistic space of random variables as

$$P_f = \int_{g(\boldsymbol{X}) \leq 0} f_x(\boldsymbol{X}) d\boldsymbol{X} \tag{2}$$

where f_x is the joint PDF of the limit state and $\boldsymbol{X}$ is the vector of random variables in g. The failure region is the probability space where $g \leq 0$. For most practical problems, it is well known that the formulation of f_x and its integration over the failure region are typically too difficult to compute directly. Therefore, numerous alternative methods have been developed to estimate P_f without the direct use of Eq. (2). In general, these methods might be classified as simulation or sampling-based methods (e.g., Monte Carlo simulation and its variants) and analytical (but numerically implemented) algorithms. The former, although potentially highly accurate, are generally plagued by a requirement for a large number of samples (i.e., evaluations of the limit-state function) to accurately estimate failure probability. Although there are some exceptions with variance reduction techniques, this problem can be expected to worsen as failure probability becomes smaller. Of the analytical approaches, the most common ones make use of the reliability index, β, as a surrogate measure of failure probability, and bypass the direct calculation of P_f entirely. Assuming β is computed accurately, it can be shown that a transformation to P_f can be made by use of the standard normal cumulative distribution function, Φ such that $P_f = \Phi(-\beta)$. Although computationally efficient, these analytical methods must be used with caution as the accuracy varies with the non-linearity of the limit state, the non-normality of the random variables, as well as other characteristics of the limit state function (Eamon et al. 2005). The necessary requirement of these

methods is to locate the most probable point of failure (MPP), which typically requires an optimization algorithm. At the MPP, the limit state is approximated with a linear or higher order formulation from which reliability index can be calculated.

For this study, the iterative Advanced Mean Value Plus (AMV+) method is used to calculate reliability index (Wu et al. 1990). This method is a variant of the first-order reliability method (FORM), or Rackwitz-Fiessler procedure (Rackwitz and Fiessler 1978). In this method, the limit state function g is repeatedly re-approximated about the MPP ($\boldsymbol{x}^*$) until convergence, but with AMV+, an additional sub-iteration is added on the linearized function that requires no calls to the true response. This usually allows the MPP to converge more quickly than the Rackwitz-Fiessler algorithm, provided that the limit state response is complex and computationally costly, as with those in this study. The specific process is as follows:

1. The limit state is linearized using a first-order Taylor series expansion at the MPP. For the first iteration, the mean values of random variables are used in place of the MPP. This step requires n+1 calls to the exact limit state function, where n is the number of random variables in the problem.

$$g = z \approx z(\boldsymbol{x}^*) + \sum_{i=1}^{n} \left(\frac{\partial z}{\partial X_i} \right)\Bigg|_{\boldsymbol{x}^*} \left(X_i - x_i^* \right) \tag{3}$$

where $z(\boldsymbol{x}^*)$ is the limit state function evaluated at the MPP and represents one call to the true response (i.e., FEA code), $\frac{\partial z}{\partial X_i} = \frac{\partial g}{\partial X_i}$ are the derivatives of the limit state function with respect to each random variable X_i. As the limit state is an implicit function of the random variables, these derivatives are calculated numerically using a finite difference procedure. The evaluation of each derivative requires one call to the true response.

2. A gradient-based optimization algorithm is used to locate the MPP of the linearized function. This sub-iteration requires no calls to the true response.

3. Steps 1 and 2 are repeated until MPP convergence. Typically, only several iterations are required for convergence. At the converged MPP, reliability index can be calculated as

$$\beta = \frac{z}{\tilde{\sigma}_z} \tag{4}$$

where

$\tilde{\sigma}_g = \sqrt{\sum_{i=1}^{n}\left(\frac{\partial z}{\partial X_i}\right)^2 \tilde{\sigma}_i^2}$ is the linearized standard deviation, which is a function of the random variable standard deviations $\tilde{\sigma}_i$:

Mathematical Formulation of the RBDO Problem

In RBDO, inherent uncertainties associated with material properties, loads, sizing, strength, and other parameters, are captured in the mathematical formulation and solution of the optimization problem. There are multiple ways of formulating an RBDO problem (Enevoldsen and Sorensen 1994, Frangopol 1995, and Tu et al. 1999). In its generic form, we seek the optimal vector of design variables $\boldsymbol{Y} = \{Y_1, Y_2, ..., Y_{NDV}\}^T$ that would

$$\begin{aligned} &\text{min} && f(\boldsymbol{X},\boldsymbol{Y}) \\ &\text{s. t.} && P_{f_i} = P\left[g_i^p(\boldsymbol{X},\boldsymbol{Y}) < 0\right] \le P_{\max}; \quad i = 1, N_p; \\ & && Y_k^l \le Y_k \le Y_k^u; \qquad k = 1,2,..., \text{NDV} \end{aligned} \tag{5}$$

where $f(\boldsymbol{X},\boldsymbol{Y})$ is the objective function of interest with dependence on design and possibly the random variables, $\boldsymbol{X} = \{X_1, X_2, ..., X_n\}^T$. Each of the N_p design constraints is expressed as a probability of failure P_{f_i} or, specifically, as the probability of limit state g_i^p becoming negative is no greater than the specified limit, $P_{\max}$. The design variables in Eq. (5) could be independent or represent the mean values of a subset of random variables, with the kth design variable, Y_k limited by its lower and upper bounds, Y_k^l and Y_k^u, respectively. For a tradeoff between design efficiency and robustness, the performance

function in Eq. (5) can be written as $f(\boldsymbol{X},\boldsymbol{Y}) = a_1\mu_f(\boldsymbol{X},\boldsymbol{Y}) + a_2\tilde{\sigma}_f(\boldsymbol{X},\boldsymbol{Y})$, where μ_f and $\tilde{\sigma}_f$ represent the mean and standard deviation values, respectively, of the objective function, and coefficients a_1 and a_2 denote scalar weighting factors that signify the desired emphasis on efficiency and robustness, respectively (Rao 1992).

By using the relationship between failure probability P_f and reliability index β, it is possible to express the constraint limit in terms of the corresponding target or minimum reliability index as $\beta_{\min} \approx -\Phi^{-1}(P_{\max})$. This relationship between P_f and β is exact when β is computed for linear limit states containing normally distributed random variables. As noted above, for nonlinear limit states, some accuracy is lost if a translation back to P_f is desired, although for typical problems, β usually provides acceptable accuracy.

As is often the case, some responses such as structural weight may be marginally impacted or totally unaffected by the variability in the random variables (i.e., design uncertainties), and consequently they can be treated as deterministic. With weight as the objective function and a subset of design constraints as deterministic, Eq. (5) can be rewritten as

$$
\begin{aligned}
\text{min} \quad & f(\boldsymbol{Y}) = W(\boldsymbol{Y}) \\
\text{s.t.} \quad & \hat{g}_i^p(\boldsymbol{X},\boldsymbol{Y}) = \frac{P\left[g_i^p(\boldsymbol{X},\boldsymbol{Y}) \le 0\right]}{\Phi(-\beta_{\min})} - 1 \le 0; \qquad i = 1, N_p \\
& \hat{g}_j^d(\mu_{\boldsymbol{X}},\boldsymbol{Y}) = \frac{R_j(\mu_{\boldsymbol{X}},\boldsymbol{Y})}{R_{j_{\max}}} - 1 \le 0; \qquad j = 1 \text{ to } N_d \\
& Y_k^l \le Y_k \le Y_k^u; \qquad k = 1 \text{ to } NDV
\end{aligned}
\tag{6}
$$

where $\hat{g}_i^p$ and $\hat{g}_j^d$ represent normalized reliability-based and deterministic constraints, respectively, with the latter preventing the critical value of a deterministic response, R_j from exceeding its maximum allowable value, $R_{j_{\max}}$. In Eqs. (6), N_p and N_d represent the number of probabilistic and deterministic constraints, respectively.

The presence of probabilistic design constraints makes the solution of Eq. (6) challenging and expensive. Different approaches for the evaluation of $\hat{g}_i^p(\boldsymbol{X},\boldsymbol{Y})$ have been developed. In the reliability index approach (Enevoldsen and Sorensen 1994), $\hat{g}_i^p(\boldsymbol{X},\boldsymbol{Y})$ is described in terms of a lower bound on the reliability index (i.e., $\hat{g}_i^p(\boldsymbol{X},\boldsymbol{Y}) = 1 - \beta_i(\boldsymbol{X},\boldsymbol{Y}) \big/ \beta_{\min_i} \le 0$, where $\beta_i(\boldsymbol{X},\boldsymbol{Y}) = -\Phi^{-1}\left(P\left[g_i^p(\boldsymbol{X},\boldsymbol{Y}) \le 0\right]\right)$) whereas in the performance measure approach (Tu et al. 1999), it is modeled using inverse transformation (i.e., $\hat{g}_i^p(\boldsymbol{X},\boldsymbol{Y}) = -F_{G_i}^{-1}\left(\Phi(-\beta_{\min_i})\right) \le 0$, where $F_{G_i}(0) = P\left[g_i^p(\boldsymbol{X},\boldsymbol{Y}) \le 0\right]$). More recently, Du and Chen (2004) proposed the replacement of $\hat{g}_i^p(\boldsymbol{X},\boldsymbol{Y})$ with an equivalent deterministic constraint and the decoupling of reliability analysis and design optimization in each design cycle whereas Qu and Haftka (2004) suggested the use of probability safety factor in modeling of each probabilistic constraint.

The specific details regarding the application of RBDO to a complex marine structure are presented next.

Composite Submarine Sail Structure

A new design concept envisioned for the next-generation Navy submarines replaces the current airfoil shaped sail with a canopy style configuration known as the Composite Advanced Sail (CAS) and shown in Fig. 1. The CAS concept is aimed at enhancing the performance of the submarine while increasing its payload capacity. Considering the length, width, and height dimensions of approximately 100 x 20 x 20 ft, together with large-size stiffeners and a thick outer shell, structural weight is a major concern. To reduce weight and maintenance costs, the new sail design will be primarily made of glass-reinforced polymer (GRP) composite materials.

Earlier efforts in structural design were based on a parametric study (Sprecace 2000) to examine the effects of alternative stiffener layouts and the subsequent nonlinear FEA studies (Cowan 2001) for various load cases. The baseline CAS model with one longitudinal and ten transverse stiffeners was optimized for minimum weight using a deterministic formulation and solution of the sizing optimization problem (Rais-Rohani et al. 2005). Subsequent reinforcement layout (topology) and sizing optimization

(Rais-Rohani and Lokits 2006) resulted in a new optimal design with approximately 19% weight savings over the original baseline CAS. The revised stiffener layout with 2 longitudinal and eight transverse stiffeners is shown in Fig. 2.

The deterministically optimized CAS (Rais-Rohani and Lokits 2006) represents a significant design improvement, in terms of material usage and the internal stiffener geometry. However, revisions of this magnitude are typically accompanied by performance uncertainties. To quantify these uncertainties, a reliability analysis was conducted (Eamon and Rais-Rohani 2008), which indicated considerable differences in reliability among the various structural components of the deterministic-optimum design model. Due to these differences, as well as the low reliability indices of some components, the CAS optimization problem represents an excellent candidate for sizing optimization under RBDO methodology.

CAS Model Description

Because of variation in material composition, the CAS outer shell is divided into four separate components: the crown, transition, main, and base joint (see Fig. 1). Whereas the crown is made of a thick layer of steel, the transition and main skin regions are made of laminated composite materials with bi-directional fabric GRP (FGRP) layers of either $\pm 45°$ or $0/90°$ orientation. The same FGRP plies that are in the main skin extend into the base joint and are sandwiched between two steel plates of different thickness to accommodate a rigid attachment to the pressure hull. The transition region serves as an interface between the crown and main skin regions. Given the large size of the structure and severity of external loads, the outer shell of CAS could reach several inches in thickness.

To support the applied load, the laminated skin is stiffened by ten additional components: two longitudinal and eight transverse stiffeners in the shape of a closed hat section. As shown in Fig. 2, five transverse stiffeners (TS1, TS2, TS6, TS7, and TS8) extend from the base joint boundary on one side to the other whereas the remaining three (TS3, TS4, and TS5) are terminated at the boundary line between

the transition and main skin regions. The stiffeners consist of a base laminate of $\pm 45°$ FGRP layers with additional unidirectional GRP (UGRP) layers in the cap portions.

The laminate composition and material system are summarized in Table 1. For simplicity, the GRP laminate composition is modeled with few thick and thin layers of consistent orientation angles. The thick layers, denoted by symbol *d*, are allowed to change thickness during design optimization whereas the thin layers, denoted by *t*, are kept at constant thickness. The thin layers offer negligible strength and stiffness to the laminate and are used only as means of strain recovery at a more critical inter-laminar surface as opposed to mid-ply location of underlying thick layer of the same material properties and orientation angle. The choice of subscripts for the *d* layers in Table 1 is meant to show that while the thickness of $\pm 45°$ and $0/90°$ FGRP layers in the same laminate are kept equal, thickness dimension can vary from one member to another. This is to maintain quasi-isotropic properties in each laminate while offering the optimizer greater flexibility to reduce the overall weight of the structure by tailoring the wall thickness in different regions per the specified structural requirements. Although thickness of steel crown is allowed to change, the steel plates in the base joint are kept at constant thickness as denoted by h_{st_1} and h_{st_2} in Table 1.

Here, the thickness of thick layers in each laminate together with the thickness of crown region form the vector of design variables. Considering the number of stiffeners, separation of flange, web, and cap portions into independent laminates, and the three regions of the outer skin, the total number of design variables in the CAS RBDO model comes to 43. While ply thickness is allowed to change during the optimization process, the corresponding laminate ply pattern is kept fixed as indicated in Table 1. The listing of design variables Y_1 to Y_{43} is given in Table 2. The normalized initial values in Table 2 represent the normalized optimal values obtained through deterministic optimization of the CAS model (Rais-Rohani et al. 2006). For the CAS RBDO problem, the lower and upper bounds for Y_1 to Y_{42} are taken as $0.5Y_k^I$ and $2.0Y_k^I$, respectively, where Y_k^I is the initial value of the kth design variable. For

Y_{43},the bounds are taken as Y_{43}^{I} and $2.0\,Y_{43}^{I}$. The lower bounds represent the minimum thickness necessary to satisfy other design constraints besides those considered in the RBDO problem.

The FE model of CAS as shown in Fig. 2 consists of approximately 18,600 four-node quadrilateral and 350 three-node triangular shell elements paired with a material model that allows the discrete modeling of individual layer properties. In addition to the outer surface, the webs, flanges, and caps of the stiffeners are also discretely modeled as shell elements. The entire model has 96,700 degrees of freedom. The base boundary of the CAS is constrained with a fixed boundary condition, representing its rigid attachment to the submarine hull. The transient wave-slap, caused by an ocean wave striking the sail on one side, is taken as the most critical load, and is modeled by an equivalent static load (uniform pressure) on the port side of the sail (Cowan 2001). Both steel and GRP composite materials are modeled as linear elastic. While the strength limit for the steel material is measured using von Mises criterion, that of GRP is measured using the maximum strain based on the first-ply failure criterion of laminated composite materials. Consequently, linear static FEA is used to determine the static strength of the structure while a buckling eigenvalue solution is used to find its elastic stability.

Design Constraints in CAS RBDO

In order to identify the reliability-based and deterministic set of design constraints, a reliability analysis of the deterministic-optimum CAS design was conducted with details presented in (Rais-Rohani et al. 2006). However, for completeness sake, an overview of the selection process is described in this section.

Reliability is measured in terms of component failure. There are 14 primary sail structural components in the reliability model: the crown, main, transition, and base-joint skin along with ten stiffeners. As noted above, most components are made of multiple GRP layers. Currently, no data are available regarding material layer correlations. However, as described in Rais-Rohani et al. (2006), a negligible difference in reliability was found between the fully correlated and uncorrelated material layer models. Thus, full correlation among layer properties for a particular material type (FGRP, UGRP) within a component is assumed, which greatly reduces computational effort from the uncorrelated case. For the

thin GRP plies making up the strain recovery layers (see Table 1), a separate limit state is formulated for each strain component in the principal material directions. These limit states are expressed generically as

$$g_1 = \varepsilon_{tx_{\max}} - \varepsilon_{tx} \tag{7}$$

$$g_2 = \varepsilon_{cx_{\max}} - \varepsilon_{cx} \tag{8}$$

$$g_3 = \varepsilon_{ty_{\max}} - \varepsilon_{ty} \tag{9}$$

$$g_4 = \varepsilon_{cy_{\max}} - \varepsilon_{cy} \tag{10}$$

$$g_5 = \gamma_{\max} - \gamma \tag{11}$$

where ε_{tx} and ε_{cx} are the axial tensile and compressive strains, respectively, in the fiber direction whereas ε_{ty} and ε_{cy} are the axial tensile and compressive strains, respectively, in the transverse direction, with γ representing the in-plane shear strain. These strains are calculated from FEA of the CAS with upper bounds equal to material allowable values. Limit states in Eqs. (7)-(11) apply to FGRP and UGRP strain-recovery layers of the stiffeners as well as the FGRP strain-recovery layers in transition, main and base joint regions of the skin. In addition, a limit on von Mises strain in the crown region and another on buckling load factor of the whole structure brings the total number of potential limit states to 117.

The initial set of resistance random variables included four material stiffness parameters and five material strength parameters with statistical properties described in Table 4. The GRP random variables are the elastic moduli in the principal material directions (E_{xx}, E_{yy}), shear modulus (G_{xy}), Poisson's ratio (ν_{xy}), the allowable tensile strains in each direction ($\varepsilon_{tx_{\max}}, \varepsilon_{ty_{\max}}$), the allowable compressive strains ($\varepsilon_{cx_{\max}}, \varepsilon_{cy_{\max}}$), and the allowable in-plane shear strain ($\gamma_{\max}$). For the steel crown, the random variable is taken as the allowable von Mises strain, $\varepsilon_{st\,max}$. In addition, there is a load random variable, live load pressure (*LL*). Based on the results of reliability analysis of GRP structures in a previous study (Thompson et al. 2005), material thickness variability is deemed insignificant and not included here. Separating all $\pm 45°$ FGRP layers, all $0/90°$ FGRP layers, all UGRP layers, and the steel parts regardless of component into separate groups, and assuming each group has an independent set of material

properties, we find a total of 205 random variables in this system.

Although it is possible that some degree of correlation exists among the material property random variables, no relevant data are yet available. Thus, they are currently assumed to be uncorrelated. Mean maximum wave-slap load over the CAS design lifetime (30 years) is based on the available load data while the corresponding coefficient of variation (COV) is based on an analysis of wave energy (Ozger et al. 2004) found from ocean buoy data (NDBC 2005). All random variables are assumed to have a normal probability distribution (Rais-Rohani et al. 2006).

The reliability analysis of the deterministic-optimum CAS model showed that the limit state on shear strain of FGRP layers in transverse stiffeners (TS) generally had the lowest reliability index values, with $\beta_{TS5} = 1.84$, $\beta_{TS1} = 2.32$, $\beta_{TS7} = 3.29$, $\beta_{TS4} = 3.84$, $\beta_{TS2} = 3.98$, and $\beta_{TS6} = 4.05$ representing the lowest six beta values. Other low strength reliability indices were associated with von Mises strain in the crown (CR) ($\beta_{CR} = 2.09$), and axial tension strain of UGRP in TS7 ($\beta_{TS7u} = 3.97$). As reference, a reliability index of 2.33 translates into an approximate failure probability of 0.01 for the corresponding limit state. The remaining material strength limit states, of the 116 total considered for the entire structure, had substantially higher reliability indices ranging from 5.08 to greater than 10. Basing the reliability of the CAS structural system on a first-component failure (series system) model, the few lowest component reliability indices govern system performance.

The reliability index for the first buckling mode of the deterministic-optimum CAS design was found to be 2.51. Using this value as the lowest acceptable component reliability index, the minimum reliability indices of the lowest, most critical constraints are set equal to 2.51 while the remaining strength constraints are treated as deterministic with bounds given in Table 3. Although buckling is an important failure mode, it is not directly included in the RBDO due to its associated computational expense. However, buckling performance is considered as part of the post-RBDO evaluation discussed later.

Hence, the critical set of limit states to be treated as reliability-based design constraints is reduced to the following three

$$g_{\gamma} = \gamma_{\max} - \gamma_{\text{FP}} \tag{12}$$

$$g_{\varepsilon t} = \varepsilon_{\max} - \varepsilon_{\text{UP}} \tag{13}$$

$$g_{cr} = \varepsilon_{\text{st}_{\max}} - \varepsilon_{\text{CR}} \tag{14}$$

where g_{γ}, $g_{\varepsilon t}$, and g_{cr} represent the limit states for shear strain in FGRP plies of skin as well as cap, web, and flange laminates of stiffeners, tensile strain in UGRP plies of stiffener caps, and von Mises strain in the steel crown region, respectively, with strain bounds as those specified in Table 3. In Eqs. (12) - (14), $\gamma_{\max}$, $\varepsilon_{\max}$, and $\varepsilon_{\text{st}_{\max}}$ represent the allowable maximum values for shear strain in FGRP plies, axial strain in UGRP plies, and von Mises strain in steel, respectively. By examining the shear and axial strains in all strain recovery layers that are made of FGRP or UGRP materials, we find the corresponding maximum values denoted by γ_{FP} and ε_{UP}. For the steel crown, ε_{CR} represents the maximum von Mises strain. The measured strain values are obtained from FE simulations as functions of material and loading random variables.

The use of a single limit state for all layers throughout the structure that are made of the same material is not meant to imply that full correlation exists among the component strengths. Rather, this is the worst-case search approach in which reliability is calculated only for a component of a particular material type (FGRP, UGRP, or steel) with the highest strain. These highest strain values become γ_{FP}, ε_{UP}, and ε_{CR} in the limit states g_{γ}, $g_{\varepsilon t}$, and g_{cr}, respectively. Since materials of the same type in all components share the same statistical parameters for strength (regardless of correlation assumption), the component with the highest load effect must necessarily have the lowest reliability index and is captured in this process. Thus, for the CAS RBBO problem, a distinct evaluation of reliability for each individual component is not needed, but rather only the minimum reliability index of any component is required. The benefit of this approach is that it greatly reduces the number of probabilistic limit states (from 117 to the three above), which is essential in managing the computationally intensive RBDO process.

In the CAS RBDO problem, both strength and stability requirements must be satisfied. For the composite components, the strength requirements are formulated using the maximum-strain failure criterion based on the first-ply failure theory of laminated composite materials. For each ply in the laminate stack of a finite element, a separate upper bound is imposed on its tensile, compressive, and in-plane shear strain values in principal material directions. With 19,880 elements having multiple GRP layers, the number of strain constraints in the optimization problem could potentially reach as high as several million. However, in the formulation and solution of the optimization problem only those constraints that are active (i.e., $g \approx 0$) or violated (i.e., $g < 0$) are used. Hence, the number of retained constraints can be significantly less than the potential maximum and can vary from one optimization cycle to another. As for structural stability, the load factor associated with the lowest buckling mode is important in the CAS design.

The CAS RBDO problem is strictly one of structural optimization with sizing design variables. Although other design considerations, such as hydrodynamic performance and manufacturing, can be included in the optimization problem, they are not considered here.

Probabilistic Sensitivity Analysis

With the help of probabilistic sensitivity analysis, we can determine the influence of uncertainty (represented by standard deviation) in each candidate random variable on the reliability index of selected limit state functions. Hence, when the effect of uncertainty is important, the parameter is treated as probabilistic; otherwise, it is treated as a deterministic parameter to reduce computational cost. The non-dimensional probabilistic sensitivity derivative of a reliability index, β with respect to standard deviation $\tilde{\sigma}_{X_i}$ of random variable, X_i can be calculated as (Madson, et al. 1986)

$$\alpha_i = \frac{\partial \beta}{\partial \tilde{\sigma}_{X_i}} \left(\frac{\tilde{\sigma}_{X_i}}{\beta} \right) \tag{15}$$

From probabilistic sensitivity analysis of CAS model, we found that all of the material stiffness random variables (i.e., E_{xx}, E_{yy}, G_{xy}, and ν_{xy}) together with most of the strength random variables have

negligible effect on the selected strength-based limit states. Removing the insignificant random variables, only four (i.e., *LL*, $\gamma_{\max}$,$\varepsilon_{\max}$, and $\varepsilon_{\mathrm{st}_{\max}}$) are necessary for inclusion in the CAS RBDO problem. Thus, each of the three probabilistic limit states in Eqs. (13) – (15) is composed of only two random variables, *LL* and the pertinent material ultimate strain value.

CAS RBDO Solution Procedure

The solution of CAS RBDO problem involves FEA of the CAS model for the evaluation of linear-static responses of interest (i.e., strains), evaluation of reliability index associated with each probabilistic design constraint, formulation and solution of an approximate optimization problem for updating the values of design variables, and the evaluation of convergence criteria for termination of this iterative process.

The mathematical programming techniques that are typically used to solve a nonlinear, constrained optimization problem, such as the one defined by Eq. (6), require gradients of the objective function and those of the retained design constraints with respect to each design variable. When the objective function and/or constraints are implicit functions of design variables, as is the case here, the sensitivity derivatives are commonly calculated using a finite difference scheme, which can significantly increase the computational cost.

The constrained optimization problem is solved using the Modified Method of Feasible Directions (MMFD) in the VisualDOC (2002) program. MSC/NASTRAN (2001) is used as the FEA solver, and the probabilistic code NESSUS (2001), which contains the AMV+ method, is used to calculate the reliability indices. The communication among the individual codes is organized and managed using the VisualScript (2002) program. Additionally, several in-house FORTRAN codes are used to facilitate the recording of appropriate analysis input and output files and searching for and extracting critical responses.

A flowchart of the general steps in a single CAS RBDO cycle is given in Figure 3. A cycle starts with the optimizer determining trial values for the design variables (DVs). Note that in the very first cycle, the initial values of design variables are used. An FEA is performed and the deterministic

constraints are evaluated. With design variables held fixed, the random variables (RVs) are perturbed and the model is analyzed for reliability. The random-variable perturbations are continued until the reliability index calculation for each probabilistic constraint is completed. Based on the gradient information from the objective and constraint functions, the MMFD algorithm establishes a usable-feasible search direction to find an improved design point. The optimizer checks the optimality and convergence criteria at that point, and if necessary, additional optimization cycles are performed until an optimum solution is found.

CAS RBDO Results

For comparison purposes, we considered two different RBDO cases. In the 3-β case, the RBDO problem, as described above, consists of 43 design variables, 8 deterministic constraints, and 3 reliability-based constraints whereas in the 1-β case, a less computationally expensive problem with 42 design variables, 10 deterministic constraints, and only one reliability-based constraint (see Table 3) is solved. In the 1-β case, crown thickness is held fixed and two of the probabilistic constraints ($\beta_{\varepsilon t}$ and β_{cr}) are taken as deterministic (i.e., converted to ε_{tx} for UGRP and ε_{st} in Table 3, respectively) while the FGRP shear strain constraint, β_{γ}, which initially had the lowest component reliability index of 1.84, is taken as probabilistic.

3- β CASE

The deterministic-optimum CAS model (Rais-Rohani et al. 2006) with a weight of 75,430 lb is chosen at the initial design for the RBDO problem. The RBDO problem required 170 CPU hours on a SUN Sparc workstation to converge in 7 cycles to an optimal design having a weight of 79,360 lb, representing a weight increase of 5%. The weight increase is due to the selected value of $\beta_{\text{min}} = 2.51$, which is higher than the level of reliability in the initial design. The only way the optimizer was able to satisfy the higher reliability level was by increasing the wall thickness, hence the higher weight. The effect that the increase in reliability has on component and system safety is discussed below. The convergence history of the objective function is shown in Figure 4.

Final design variable values, as a fraction of the original, are given in Table 2. Most plies were only mildly affected and had less than 5% change in thickness. This is because the initial design variable values were based on deterministically optimized problem. Thus, many of the design variables, which were primarily governed by the large number of deterministic constraints in the model, were close to their optimal values before the start of the RBDO process. Significant thickness gains occurred in the main skin (7%); the transition region (12%); TS4 flange (10%); LS1 flange (12%); TS5 flange (20%), cap FGRP (68%) and cap UGRP (35%); TS8 web (51%); LS2 cap UGRP (57%); and TS3 cap UGRP (77%). Although individual members experienced a minor (between 1-7%) loss of weight except TS5 and TS6, the total weight saving was more significant. The TS8 cap FGRP material loss was 21%. Losses were fairly evenly distributed among stiffener webs, caps, and flanges, but only the FGRP material was affected. Final constraint response values as well as the critical component locations are given in Table 3. As seen in the "Final-to-Bound Ratio" and "Critical Component" columns for the 3-β case, the most critical constraints in the post-RBDO CAS were ε_{cx} for FGRP in the transition region and β_{cr} (with final value = 2.51).

An interesting result can be seen in the change in design variable values, which also illustrates the difficulty in choosing optimum solutions for complex structures without rigorous mathematical guidance. At the initial design, three components had a reliability index below the imposed limit of 2.51. These included the FGRP material of TS1 and TS5 that was shear-limited (β_{TS5} = 1.84; β_{TS1} = 2.32) and the crown (β_{cr}=2.09). Although the component with the lowest initial reliability index, TS5, made significant gains in ply thickness as expected, the crown, with the next lowest reliability index, had no significant difference in material thickness. Finally, TS1, the final component with an initial reliability index less than that required, experienced a net loss of material. Apparently, the best solution to meet the minimum β constraints and yet minimize weight was to globally stiffen the structure by increasing thickness of the outer shell as well as the most significant stiffeners in this regard (i.e., TS3-5, and LS1-2). This makes sense particularly with regard to the crown, which is a large volume of material (controlled by a single

design variable) as well as relatively heavy (steel) material as compared to the lightweight composite material used elsewhere in the CAS structure.

The importance of global stiffness can also be seen in the sensitivity analysis. Normalized sensitivities of the objective function and constraints with respect to design variables are presented in Figures 5 to 8.

Figure 5 presents the sensitivities of the objective function. Clearly, the main skin thickness (Y_1) is the most critical design variable, as this represents the component with the most volume of material. In Figure 5, sensitivities are identical for the initial and optimal design models, as expected.

In Figures 6 to 8, only the design variables that significantly impact the constraint are presented. Positive values indicate that an increase in layer thickness increases the response while negative values indicate increasing thickness decreases the response. In general, the main skin (Y_1) has a strong influence on almost every constraint. Also important for most constraints is the transition region (Y_2), and the FGRP and UGRP cap material in TS5 (Y_{23} and Y_{24}, respectively). Stiffener components that appear most frequently on the graphs are TS5, TS4, and TS8. Also appearing, but less frequently, are TS3, TS7, and LS2. The remaining stiffeners are insignificant with respect to constraint sensitivity. Among the stiffeners, the cap material is most critical for most constraints, with the flange material least important. Figure 8 presents the probabilistic constraints. As the constraints $\beta_{\varepsilon t}$ and β_{cr} became inactive during the RBDO, only their initial sensitivity values are presented. For the most part, initial and optimum sensitivity values are similar.

Note that there is often no obvious link between the critical component in Table 3 and the most important design variable affecting the strain responses in that component as indicated by the sensitivity plots. For example, in Table 3, consider the ε_{ty} response in the UGRP layer for the 1-β case. Here an element in TS7 was found to govern the constraint ε_{ty}. Referring to Figure 6, this constraint was found to be most sensitive to design variables numbered 1, 11, and 32. Of these three, only one, Y_{32} appears in component TS7 (see Table 2), while the two most influential design variables, Y_1 and Y_{11}, appear in the main skin and in longitudinal stiffener LS2, respectively. Similar results can be seen for the other

constraints as well. The reason for this somewhat non-intuitive result, as discussed above, is that a design variable with significant influence on the overall structural stiffness is generally a better indicator of importance than one that corresponds to the critical component thickness itself. For example, increasing the design variable value corresponding to critical component thickness increases strength but also local stiffness, and thus attracts more force to that component, resulting in strain remaining relatively constant (and thus the sensitivity of the strain limit constraint to that design variable remains low) as compared to adjusting shell thickness everywhere, which more rapidly minimizes strain in all of the stiffeners.

1-β CASE

The 1-β case required approximately 50 CPU hours to converge in six cycles (Figure 4) to a new mass of 75,600 lb, representing an increase of approximately 0.4%. The lower final mass value as compared to the 3-β case is because the probabilistic crown constraint β_{cr} was not imposed in this case. Therefore, as the initial and final maximum crown strains are identical, as indicated in the "Final-to-Initial Ratio" column in Table 3, the crown reliability index would remain at the initial value of 2.09 (as opposed to 2.51 in the 3-β case). Final design variable values are given in Table 2. Most plies were only mildly affected and had less than 3% change in thickness.

As indicated in Table 2, plies that lost thickness were the FGRP plies in the flanges of TS1 (2% loss) and TS5 (18%). The cap material of TS8 (3%) and LS2 (1%), and the web of TS5 (7%) also experienced reductions in thickness. Plies with relatively large gains in thickness are the flange plies of TS3 and TS4 (both 6% increase), the FGRP plies in the cap of TS5 (14%) and the web of TS8 (8%). As shown in Table 3, the probabilistic FGRP shear constraint (β_γ) and the deterministic crown strain constraint, ε_{cr} were most critical, with both responses equal to the bound values. The 1-β case sensitivities are very similar to those of the 3-β case and are not presented here.

System Reliability Analysis

The CAS is a structural system composed of various components, and the reliability of this system may be altered during the optimization process. To estimate the system reliability of CAS-RBDO model,

the procedure in Rais-Rohani et al. (2006) is used. A total of 116 limit states corresponding to 14 primary structural components are considered for the structure as described in Table 5. Separating FGRP and UGRP materials in each stiffener and treating them as independent sub-components, produces a reliability model with total of 24 components. For members that are made of GRP materials, component failure is characterized by the violation ($g<0$) of any of the limit states as described in Eqs. (7) – (11). For the steel crown, a single limit state, yield (as determined by von Mises stress), is considered in place of limit states g_1 to g_5.

The probability of failure of the series system of n uncorrelated components ($\rho = 0$) for limit state j, P_{fj}, is given by

$$P_{fj} = 1 - \prod_{i=1}^{n} \left(1 - P_{fji}\right) \tag{16}$$

where P_{fji} is the failure probability of component i considering limit state j. If the components are fully correlated ($\rho = 1$), P_{fj}, is given by

$$P_{fj} = \max(P_{fji}) \tag{17}$$

When the degree of correlation is uncertain, as is the case here, a failure probability bounds can be constructed by considering both Eqs. (16) and (17), which represent upper and lower bounds, respectively. If the resulting bounds are not too wide, the results may be acceptable and the exact correlation is not needed. If the difference between the bounds is unacceptably large, a more computationally costly method may be required for a more accurate solution. Using Eqs. (16) and (17), there is a need to compute P_f for each component. This is governed by the finite element with the highest load effect within the component. The AMV+ method, as described above, is used for reliability analysis.

As noted, detailed component and limit-state specific results for the pre-RBDO CAS reliability analysis are given elsewhere (Eamon and Rais-Rohani 2008), and a complete re-computation of

individual component reliability considering each of the 116 limit states is beyond the scope of this study. However, some meaningful results can be obtained using some simplifying assumptions.

Considering the Final-to-Initial Ratio column for the 1-β case in Table 3, we find that all deterministic critical responses except that for shear strain (γ) in the UGRP were slightly below their respective initial values. Thus, reliability indices for all limit states except UGRP γ will be above initial values. For UGRP γ, the initial reliability index was very high (13.2), and lowering this reliability index by a large amount (greater than 50%) will have no impact on CAS system reliability, which is governed by indices much lower. Therefore, the decrease in reliability index associated with the small increase in response value for UGRP γ is of no consequence for system results. A similar situation exists for the 3- β case, where two additional post-RBDO critical responses were slightly higher than the initial values (ε_{tx} and ε_{cx} for FGRP). However, these initial reliability indices were also much higher than those governing CAS reliability, and thus even large decreases in reliability for these responses will not affect system results. Given these observations, post-RBDO system reliability can be conservatively estimated using Eqs. (16) and (17) by assuming all previous component reliabilities (calculated using the limit states g_1 to g_5) remain unchanged from those of the pre-RBDO CAS, with the exception of those affected (i.e., increased) by the three imposed probabilistic constraints (β_γ, $\beta_{\varepsilon t}$, and β_{cr}) with post-RBDO values given in Table 3.

A final important limit state to note is buckling. Evaluated with an FEA Euler analysis, no direct link can be obtained for buckling resistance and a single CAS component, as eigenvalues are computed for the structural system as a whole. However, as buckling anywhere in the structure is taken as failure and multiple buckling locations are possible, a series sub-system model can be developed such that each buckling mode constitutes a 'component'. Both fully-correlated and uncorrelated bounds can be developed for the buckling sub-system using Eqs. (16) and (17). The higher modes that do not significantly contribute to P_f may be truncated. It was found that no more than five modes need be

considered. Buckling load factors (eigenvalues) for the pre- and post-RBDO CAS are given in Table 6. Note that in all cases, post-RBDO buckling load factors are higher.

Using the simplifications described above, the series system reliability results are given in Table 7. Considering the entire structure with all limit states including buckling, the deterministic optimum (pre-RBDO) CAS has reliability index bounds between 1.46 and 1.84. For the 1-β case, system reliability bounds are between 1.74 and 2.09, while for the 3-β case, system bounds are between 2.10 and 2.33. Using the standard normal conversion from reliability index to failure probability, $P_f = \Phi(-\beta)$ in the 1-β case, for a 0.4% increase in mass, the decrease in system failure probability is approximately 50% (pre-RBDO: $0.034 < P_f < 0.071$; RBDO (1- β): $0.018 < P_f < 0.042$). In the 3-β case, for a 5% increase in mass, the decrease in failure probability is approximately 70% (RBDO (3- β): $0.010 < P_f < 0.018$). Of course, larger gains in reliability can be achieved by increasing the target probabilistic constraint values, at the expense of larger increases in structural mass.

Conclusion

In this paper, we presented the description of RBDO methodology and its application in design of a large and complex marine structural system under uncertainties in load intensity and material resistance characteristics. The design procedure required the direct coupling of finite element analysis, numerical design optimization, and structural reliability algorithms while considering different modes of failure in the stiffened shell structure made of both metallic and laminated GRP composite materials. Through probabilistic sensitivity analysis, critical random variables were identified. The RBDO solutions indicated that a minor increase in structural mass can significantly increase both the component and system reliabilities of the CAS structure. Moreover, the overall structural stiffness was found to be generally more significant than critical component thickness values..

The inclusion of reliability-based design constraints was found to be the most expensive part of the algorithm, where moving from one to three such constraints more than tripled the computational cost (50 CPU hours to 170 CPU hours). Thus, judicial use of the number of reliability constraints, as was done in

this study, is essential to maintain reasonable computational effort when confronted with complex reliability-based structural optimization problems.

APPENDIX: Nomenclature

a	constant in objective function
ν	Poisson ratio
AMV+	advanced mean value plus method
CAS	Composite Advanced Sail
CR	crown
cx	compression, x-direction
cy	compression, y-direction
d	composite layer that has thickness as a DV
DV	design variable
E	modulus of elasticity
FEA	finite element analysis
FGRP	fabric GRP
FP	critical FGRP strain
f_x	probability density function
g	limit state function
G	shear modulus
GRP	glass-reinforced polymer
h_{st}	steel plate layer of base joint
LL	wave slap load random variable
MMFD	Modified Method of Feasible Directions
MPP	most probable point of failure
P_f	probability of failure
R	response
RBDO	reliability-based design optimization
RV	random variable
t	composite layer used for strain recovery
TS	transverse stiffener
tx	tension, x-direction
ty	tension, y-direction
UGRP	uni-directional GRP
UP	critical UGRP strain
X	a random variable
x^*	RV values at MPP
Y	a design variable
z	standard normal (reduced) RV
α	probabilistic sensitivity
β	reliability index
γ	shear strain
ε	strain
μ	mean value
σ	standard deviation
Φ	standard normal cumulative distribution function

REFERENCES

Brown, P. W., Jordaan, I. J., Nessim, M. A., Haddara, M.R., "Optimization of Bow Plating for Icebreakers," *Journal of Ship Research*, Vol. 40, No. 1, 1996, pp. 70-78.

Cowan, A.L., "AS98T Global Analysis Summary (FY 01)," Naval Surface Warfare Center, Carderock Division, CASP-01-011, Oct 2001.

Du, X. and Chen, W., "Sequential Optimization and Reliability Assessment Method for Efficient Probabilistic Design," *Journal of Mechanical Design*, Vol. 126, No. 2, 2004, pp. 225-233.

Eamon, C. and Rais-Rohani, M., "Structural Reliability Analysis of Advanced Composite Sail," SNAME *Journal of Ship Research* (to appear June, 2008).

Eamon, C., Thompson, M., and Liu, Z., "Evaluation of Accuracy and Efficiency of some Simulation and Sampling Methods in Structural Reliability Analysis," *Structural Safety*, Vol. 27, No. 4, 2005, pp. 356-392.

Enevoldsen, I. and Sorensen, J. D., "Reliability-Based Optimization in Structural Engineering," *Structural Safety*, Vol. 15, 1994, pp. 169-196.

Frangopol, D. M., "Reliability-Based Optimum Structural Design," Probabilistic Structural Mechanics Handbook, Theory and Industrial Applications, edited by Sundararajan, C., Chapman & Hall, 1995.

Jang, C.D., Kim, H.K., and Song, H.C., "Optimum Structural Design of High-Speed Surface Effect Ships Built of Composite Materials," *Marine Technology*, Vol. 40, 2003, pp. 42-48.

Leheta, H. W. and Mansour, A. E., "Reliability-based method for optimal structural design of stiffened panels," *Marine Structures*, Vol. 10, No. 5, 1997, pp. 323-352.

Madson, H. O., Krenk, S., and Lind, N. C., Methods of Structural Safety, Prentice-Hall, Inc., New Jersey, 1986, pp. 120-123.

MSC/NASTRAN Quick Reference Guide (v 2001). (2001). MacNeal-Schwendler Corp., Los Angeles, CA, U.S.

Morandi, A.C., Das, P.K., and Faulkner, D., "An Outline of the Application of Reliability Based Techniques to Structural Design and Assessment of Submarines and Other Externally Pressurized Cylindrical Structures," *Marine Structures*, Vol. 7, 1994, pp. 173-187.

National Data Buoy Center website. www.ndbc.noaa.gov. 2005

NESSUS Theoretical Manual. October 2001, Southwest Research Institute, San Antonio, TX.

Ozger, M, Altunkaynak, A., and Sen, Z., "Statistical Investigation of Wave Energy and its Reliability," Energy Conversion and Management, Vol. 45, 2004, pp. 2173-2185.

Pu, Y., Das, P.K., Faulkner, D. "Strategy for reliability-based optimization," *Engineering Structures*, Vol. 19, No. 3, 1997, pp. 276-282.

Qu, X. and Haftka, R. T., "Reliability-Based Design Optimization Using Probabilistic Safety Factor," *Structural and Multidisciplinary Optimization*, Vol. 27, No. 5, 2004, pp. 314-325.

Rackwitz, R. and Fiessler, B. "Structural Reliability Under Combined Random Load Sequence," *Computers and Structures*, No. 9, 1978.

Rais-Rohani, M., Eamon, C., and Keesecker, A., "Structural Analysis and Sizing Optimization of a Composite Advanced Sail Design Concept," *Marine Technology*, Vol. 42, No. 2, 2005, pp 61-70.

Rais-Rohani, M., Eamon, C., Lokits, J., Telegadas, H., and Bonanni, D., "Structural Analysis and Optimization of Composite Advanced Sail Design Concepts for Virginia-Class Submarines," NSWCCD-65-TR-2006/01, Naval Surface Warfare Center Carderock Division, Jan 2006.

Rais-Rohani, M. and Lokits, J., "Reinforcement Layout and Sizing Optimization of Composite Submarine Sail Structures," *Structural and Multidisciplinary Optimization*, Vol. 34, No. 1, 2007, pp. 75-90.

Rao, S.S., Reliability-Based Design, McGraw-Hill, Inc., 1992.

Rao, S.S., Engineering Optimization Theory and Practice, 3rd Ed., John Wiley & Sons, Inc., 1996.

Sprecace, A., "Parametric Analyses of Stiffening Arrangements for the ATSOL 12 Advanced Sail," Naval Surface Warfare Center Carderock Division, Contract Rept. CASP-01-01, 2000.

Thompson, M., Eamon, C., and Rais-Rohani, M., "Reliability-Based Optimization of Composite Bridge Decks," ASCE *Journal of Structural Engineering*, Vol. 132, No. 12, 2006, pp. 1898-1906.

Tu, J., Choi, K. K., and Park, Y. H., "A New Study on Reliability Based Design Optimization," *Journal of Mechanical Design*, Vol. 121, No. 4, 1999, pp. 557–564.

Wu, Y.-T., Millwater, H. R., and Cruse, T. A., "An Advanced Probabilistic Structural Analysis Method for Implicit Performance Functions," *AIAA Journal*, Vol. 28, No. 9, 1990, pp. 1840-1845.

List of Tables

List of Figures

Table 1. Material systems for the skin and stiffeners in CAS finite element model

Structural Part	Material System	Laminate Composition	Thickness
Crown	Steel	Single Layer	d_C
Transition	FGRP	$[0\text{-}90/0\text{-}90/\pm45/\pm45/0\text{-}90]_S$	$[t/d_T/t/d_T/t]_s$
Main	FGRP	$[0\text{-}90/0\text{-}90/\pm45/\pm45/0\text{-}90]_S$	$[t/d_M/t/d_M/t]_s$
Base Joint	Steel/FGRP/Steel	[ST/0-90/0-90/±45/±45/0-90/0-90/±45/±45/0-90/0-90/ST]	$[h_{st1}/t/d_B/t/d_B/t/t/d_B/t/d_B/t/h_{st2}]$
Stiffener Flange	FGRP	$[\pm45/\pm45/\pm45/\pm45/\pm45]_S$	$[t/d_f/t/d_f/t]_s$
Stiffener Web	FGRP	$[\pm45/\pm45/\pm45/\pm45/\pm45]_S$	$[t/d_w/t/d_w/t]_s$
Stiffener Cap	FGRP & UGRP	$[\pm45/\pm45/0/0/\pm45/\pm45/\pm45]_S$	$[t/d_{c1}/t/d_{c2}/t/d_{c1}/t]_s$

Table 2. Listing of Design Variables and Corresponding Values

Label	Designed part	DV	Normalized Initial Value	Final-to-Initial ratio	
				1-β case	3-β case
MS	Main Skin	Y_1	0.85	1.00	1.07
Transition	Skin	Y_2	0.78	1.04	1.12
TS 1	Flange	Y_3	0.07	0.98	0.93
	Web	Y_4	0.22	1.03	0.96
	Cap FGRP	Y_5	0.29	1.03	1.00
	Cap UGRP	Y_6	0.14	1.04	1.00
TS 2	Flange	Y_7	0.20	1.03	0.99
	Web	Y_8	0.20	1.01	0.96
	Cap FGRP	Y_9	0.48	1.00	1.00
	Cap UGRP	Y_{10}	0.32	1.01	1.03
LS 2	Cap UGRP	Y_{11}	0.19	0.99	1.57
TS 3	Flange	Y_{12}	0.30	1.06	0.97
	Web	Y_{13}	0.35	1.02	1.01
	Cap FGRP	Y_{14}	0.47	1.01	1.03
	Cap UGRP	Y_{15}	0.23	1.02	1.77
LS 1	Cap UGRP	Y_{16}	0.13	1.02	1.04
TS 4	Flange	Y_{17}	0.23	1.06	1.10
	Web	Y_{18}	0.23	1.01	0.94
	Cap FGRP	Y_{19}	0.65	1.02	0.97
	Cap UGRP	Y_{20}	0.44	1.02	1.09
TS 5	Flange	Y_{21}	0.39	0.82	1.20
	Web	Y_{22}	0.39	0.93	1.02
	Cap FGRP	Y_{23}	0.40	1.14	1.68
	Cap UGRP	Y_{24}	0.30	1.00	1.35
TS 6	Flange	Y_{25}	0.60	1.00	1.00
	Web	Y_{26}	0.60	1.02	1.04
	Cap FGRP	Y_{27}	1.00	1.03	1.05
	Cap UGRP	Y_{28}	0.70	1.03	1.03
TS 7	Flange	Y_{29}	0.70	1.00	0.98
	Web	Y_{30}	0.53	1.00	1.01
	Cap FGRP	Y_{31}	1.00	1.00	0.98
	Cap UGRP	Y_{32}	0.71	1.05	1.01
TS 8	Flange	Y_{33}	0.25	1.00	0.99
	Web	Y_{34}	0.36	1.08	1.51
	Cap FGRP	Y_{35}	0.94	0.97	0.79
	Cap UGRP	Y_{36}	0.63	1.01	1.06
LS 1	Flange	Y_{37}	0.06	1.04	1.12
	Web	Y_{38}	0.14	1.02	1.07
	Cap FGRP	Y_{39}	0.18	1.02	0.93
LS 2	Flange	Y_{40}	0.35	1.00	1.00
	Web	Y_{41}	0.34	1.02	0.99
	Cap FGRP	Y_{42}	0.41	1.02	1.00
Crown	Skin	Y_{43}	0.42	--	1.00

Table 3. Listing of Properties Treated as Design Constraints

Deterministic Constraints									
Property	Lower Bound	Upper Bound	Initial Value	RBDO (3-β)*			RBDO (1-β)*		
				Final-to-Bound Ratio	Final-to-Initial Ratio	Critical Comp.	Final-to-Bound Ratio	Final-to-Initial Ratio	Critical Comp.
UGRP (in stiffener caps)									
ε_{tx}	none	0.00685	0.0066	--	--	--	0.94	0.98	TS7
ε_{ty}	none	0.00685	0.0055	0.71	0.89	TS6	0.79	0.98	TS7
ε_{cx}	-0.0057	none	-0.0049	0.79	0.90	TS4	0.86	0.99	TS4
ε_{cy}	-0.0057	none	-0.0040	0.61	0.88	TS1	0.69	0.99	TS2
γ	-0.0114	0.0114	0.0041	0. 33	1.12	TS8	0.37	1.02	TS8
FGRP (in skin and stiffeners)									
ε_{tx}	none	0.00685	0.0060 (0.0048)	0.94 (0.57)	1.06 (0.81)	transition (TS4)	0.87 (0.70)	0.99 (0.99)	main skin (TS3)
ε_{ty}	none	0.00685	0.0057 (0.0048)	0.74 (0.66)	0.88 (0.94)	main skin (TS4)	0.83 (0.69)	0.99 (0.99)	main skin (TS4)
ε_{cx}	-0.00587	none	-0.0058 (-0.0056)	1.00 (0.79)	1.04 (0.92)	transition (TS3)	0.98 (0.91)	0.95 (0.98)	main skin (TS8)
ε_{cy}	-0.00587	none	-0.0056 (-0.0051)	0.91 (0.79)	1.00 (0.85)	main skin (TS3)	0.95 (0.85)	0.97 (0.99)	main skin (TS3)
Steel (Crown)									
ε_{st}	none	0.00210	0.00210	--	--	--	1.00	1.00	crown

Probabilistic Constraints							
Property	Lower Bound	Upper Bound	Initial Value	RBDO (3-β)		RBDO (1-β)	
				Final Value	Critical Comp.	Final Value	Critical Comp.
β_{γ}	2.51	none	1.84	3.20	TS5	2.51	TS5
β_{st}	2.51	none	3.97	4.19	TS7	--	--
β_{cr}	2.51	none	2.09	2.51	crown	--	--

*Numbers in parentheses refer to results considering components 1-10 (i.e. the stiffeners) only while the upper number (without parentheses) considers results from all components including crown, main skin, and transition region.

Table 4. Statistical Properties of Random Variables

	FGRP			UGRP		
RV	mean	COV	distribution	mean	COV	distribution
E_{xx}*	3.50e6 psi	0.055	normal	5.53e6 psi	0.055	normal
E_{yy}*	3.50e6 psi	0.055	normal	1.42e6 psi	0.055	normal
G_{xy}*	5.0e5 psi	0.003	normal	5.0e5 psi	0.003	normal
v_{xy}*	0.098901	0.003	normal	0.2424	0.003	normal
$\varepsilon_{tx_{\max}}$ or $\varepsilon_{ty_{\max}}$	0.0138	0.065	normal	0.012	0.065	normal
$\varepsilon_{cx_{\max}}$ or $\varepsilon_{cy_{\max}}$	-0.0121	0.050	normal	-0.010	0.050	normal
$\gamma_{\max}$	0.015	0.015	normal	0.015	0.015	normal
		Other				
LL	λ=2.28**	0.167	normal			
$E_{\text{st max}}$*	2.96e6 psi	0.01	normal			
v_{st}*	0.30	0.026	normal			
$\varepsilon_{st_{\max}}$	0.00290	0.05	lognormal			

*These RVs were found to be insignificant in the probabilistic sensitivity analysis and hence were excluded in the RBDO solutions.

**Bias factor (ratio of mean to nominal) is given. Load magnitude is comparable to hurricane-level wind pressure, but exact value is not available for public release.

Table 5. Components and Limit States

Comp #	Component Name	Material Sub-Components	Limit States Considered	Total # of Limit States per Component
1-10	Stiffener 1-10	FGRP, UGRP	g_1-g_5, g_1-g_5	10 (x 10 stiffeners)
11	Transition	FGRP	g_1-g_5	5
12	Main Skin	FGRP	g_1-g_5	5
13	Crown	Steel	yield	1
14	Base Joint	FGRP	g_1-g_5	5
		Total # of Limit States:		116

Table 6. Buckling Load Factors for Different CAS Designs

Mode	Pre-RBDO	RBDO (1-β)	RBDO (3-β)
1	1.42	1.45	1.72
2	1.44	1.49	1.77
3	1.55	1.60	1.79
4	1.67	1.67	1.85
5	1.77	1.84	1.87

Table 7. Estimated System Reliability Indices

Subsystem Considered in CAS	Pre-RBDO		RBDO (1-β)		RBDO (3-β)	
	$\beta, \rho = 0$	$\beta, \rho = 1$	$\beta, \rho = 0$	$\beta, \rho = 1$	$\beta, \rho = 0$	$\beta, \rho = 1$
all components 1-14 (g_1-g_5)	1.54	1.84	1.80	2.09	2.10	2.33
buckling	2.29	2.52	2.55	2.69	4.23	4.31
all components + buckling	1.46	1.84	1.74	2.09	2.10	2.33

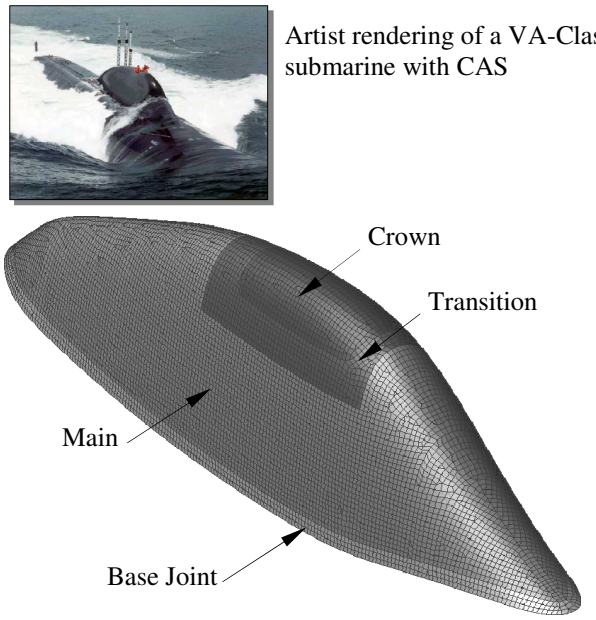

Figure 1. Conceptual model of the CAS.

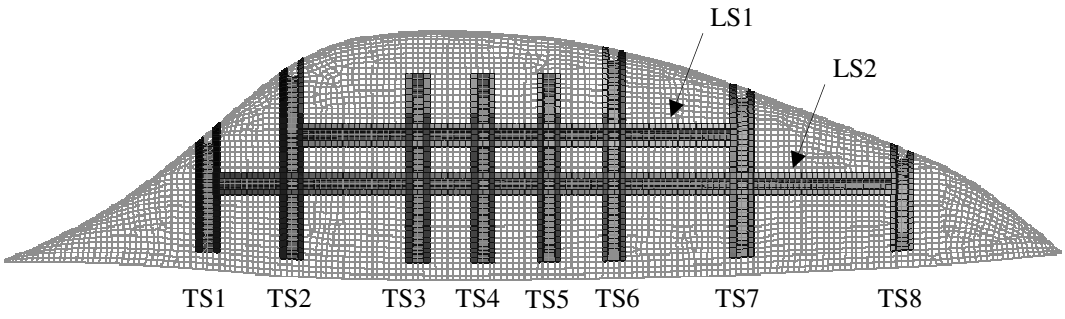

Figure 2. Finite element model of the CAS with highlighted stiffener layout

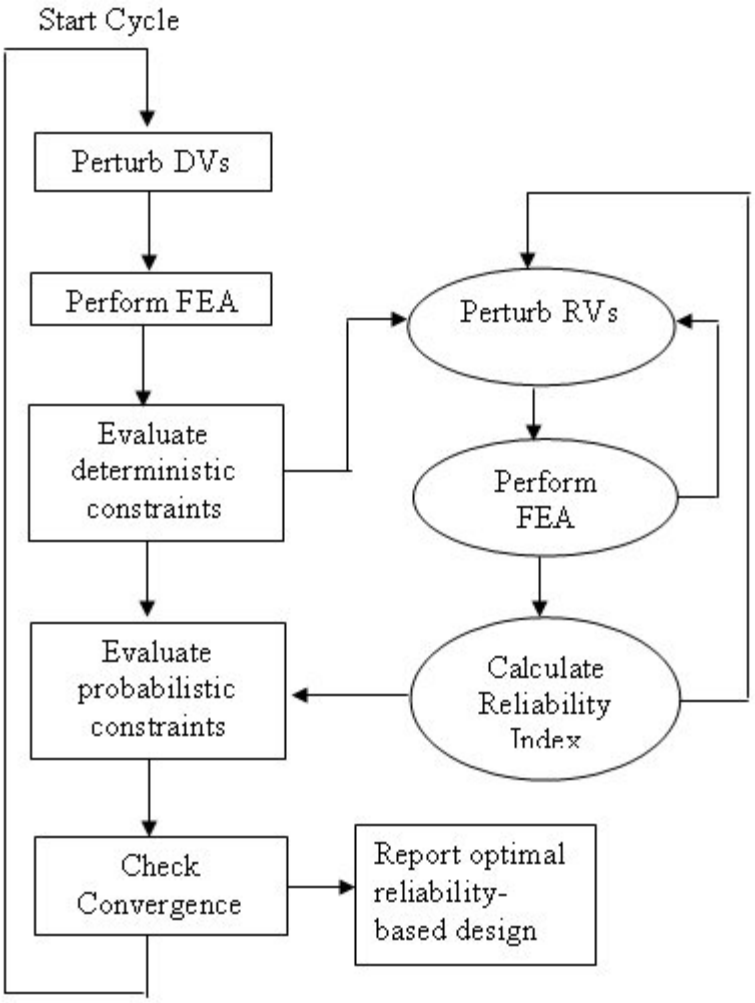

Figure 3. CAS RBDO flowchart

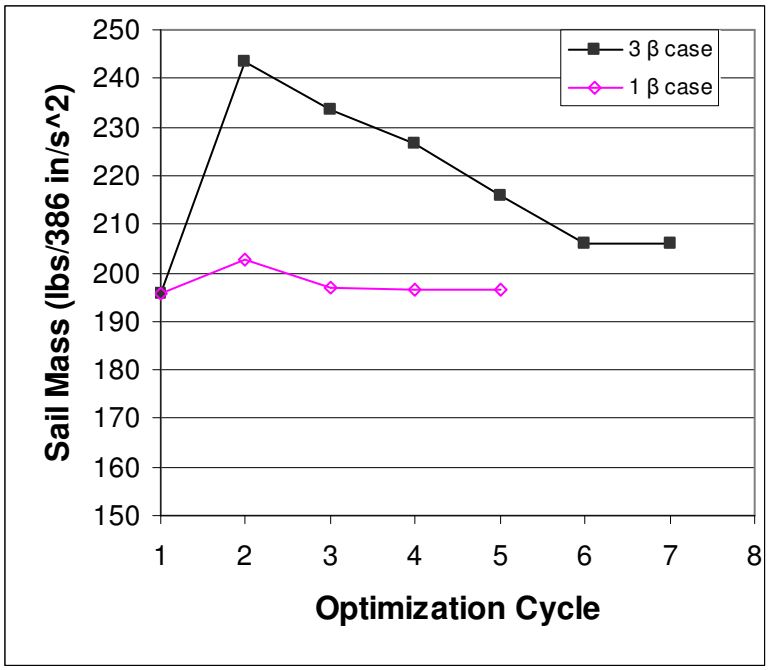

Figure 4. Convergence history

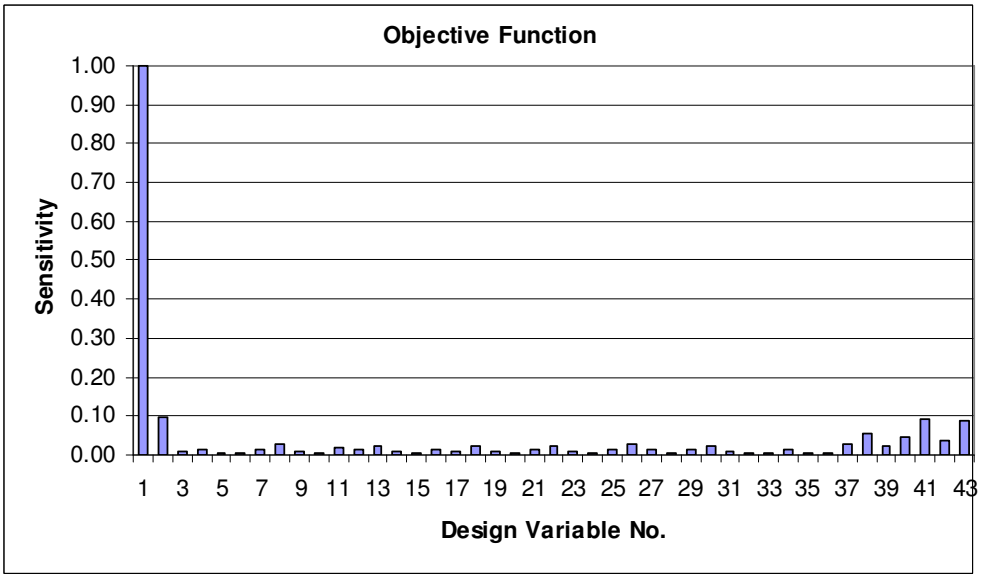

Figure 5. Normalized sensitivities of CAS weight with respect to design variables.

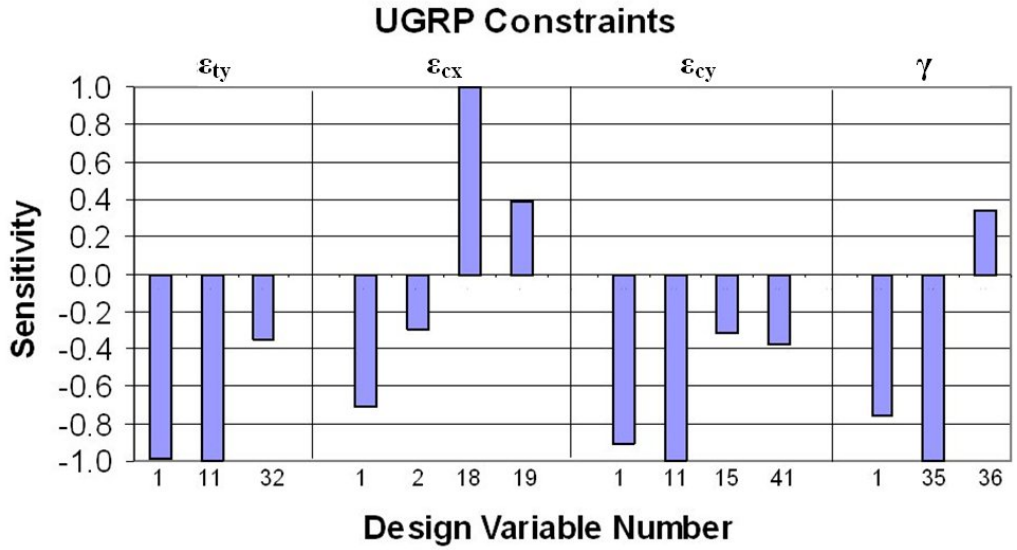

Figure 6. Normalized sensitivities of deterministic UGRP constraints with respect to significant design variables.

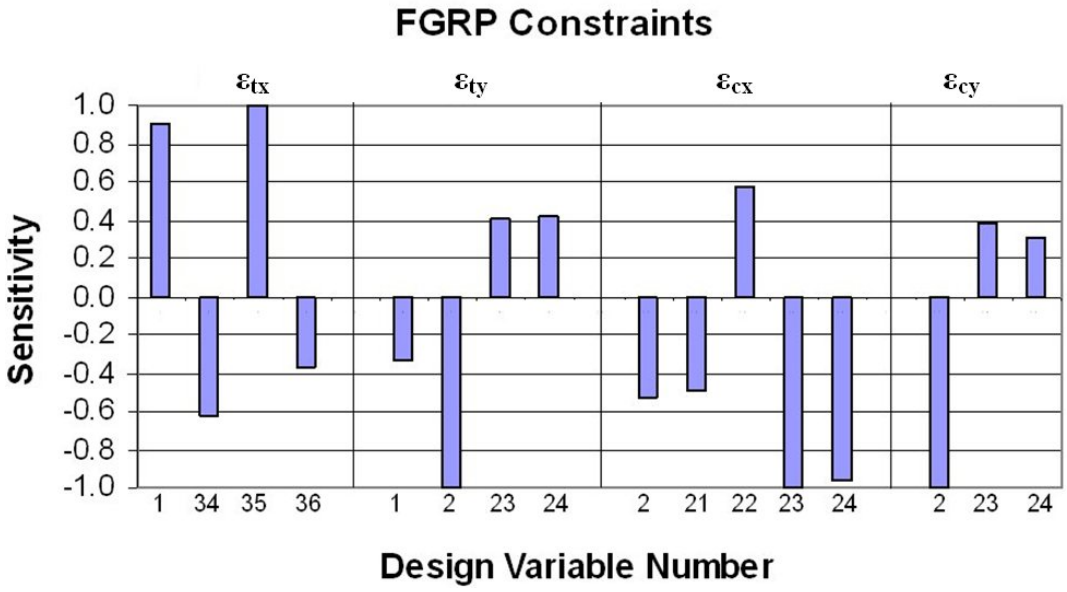

Figure 7. Normalized sensitivities of deterministic FGRP constraints with respect to significant design variables.

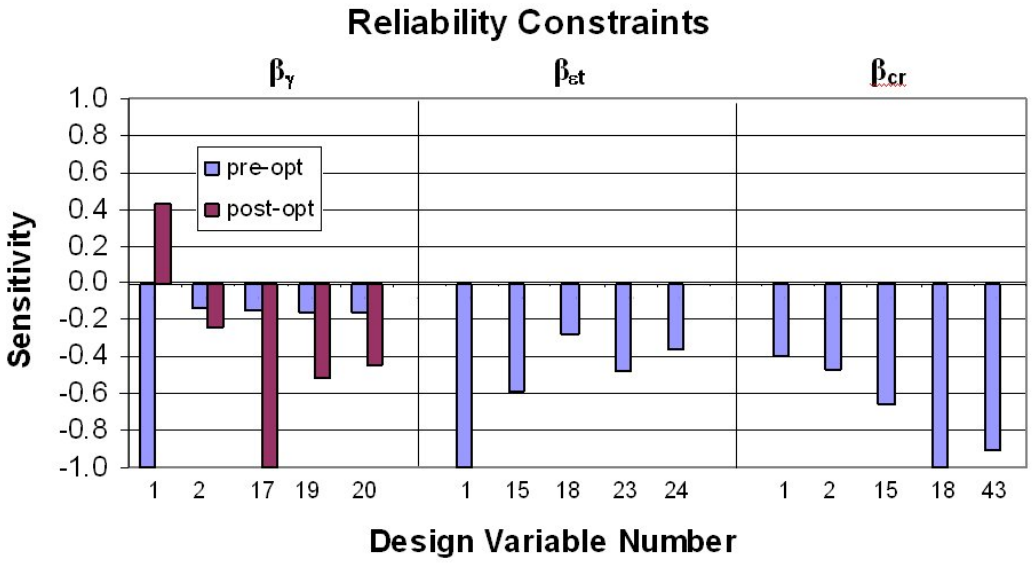

Figure 8. Normalized sensitivities of probabilistic constraints with respect to significant design variables.